

Mechanistic aspects of the formation of carbon-nanofibers on the surface of Ni foam: A new microstructured catalyst support

Nabeel A. Jarrah, Jan G. van Ommen, Leon Lefferts *

Catalytic Processes and Materials, Faculty of Science and Technology, IMPACT, University of Twente, PO Box 217, 7500 AE, Enschede, The Netherlands

Received 21 November 2005; revised 14 February 2006; accepted 25 February 2006

Available online 24 March 2006

Abstract

This paper describes the catalytic formation of a layer of carbon nanofibers (CNFs) on Ni foam, resulting in a new catalytic route for preparing thin, highly macroporous layers. The effect of morphology and surface properties (i.e., grain size and presence of NiO) on the rate formation and properties of CNFs is explored. The formation of CNFs on polycrystalline Ni starts with the formation of metastable Ni_3C , which later decomposes into Ni and C. As a result, Ni nanoparticles are created with a suitable size (20–70 nm) to catalyze the formation of CNFs. The formation of CNFs on polycrystalline Ni reveals an inhibition time in accordance with the formation and decomposition of Ni_3C resulting in Ni nanoparticles necessary for the growth of CNFs. Grain boundaries in the parent Ni material appear to enhance this process. The presence of NiO increases the formation rate of CNFs by one order of magnitude. NiO is reduced in situ, and Ni nanoparticles are formed directly, as opposed to sluggish formation of Ni nanoparticles via decomposition of Ni_3C particles formed from relatively large (1–10 μm) Ni crystals.

© 2006 Elsevier Inc. All rights reserved.

Keywords: Carbon nanofibers; Ni foam; Microstructured catalyst; Mechanism

1. Introduction

Carbon nanofibers (CNFs) are graphite materials that can be formed via catalytic decomposition of hydrocarbons or CO over small metal particles, such as Ni [1]. CNF formation is considered a serious problem in catalytic reactors because they are formed in a temperature range in which many important metal-catalyzed reactions, including Fisher–Tropsch synthesis and steam reforming, are carried out. CNFs are mechanically strong, so that the formation of these materials not only destroys the catalyst, but also may even damage the reactor wall [2]. Moreover, formation of CNFs causes an increase in the pressure drop and reduction of heat transfer properties from fouling in reactors and heat exchangers, respectively [3–5].

Baker [6] and Geus [7] turned this nuisance into an opportunity by making CNFs and carbon nanotubes (CNTs) in the same way on purpose. The bucky-ball type of preparation of thin CNTs and eventually single-walled tubes was initiated by

Iijima [8]. It is important to note that these preparation methods differ dramatically. The catalytic preparation uses relatively low temperatures and simple chemicals, such as supported Fe, Ni, or Co catalysts and a hydrocarbon or CO. The resulting CNFs and CNTs are generally more defective and often thicker than the materials obtained with arc-discharge, laser ablation, or chemical vapor deposition at very high temperatures. These latter methods are much more expensive; moreover the yield of CNTs and CNFs is generally low, and amorphous carbon must be removed. In many cases metallic catalyst precursors are used in these syntheses as well, suggesting similarities in the growth mechanism.

CNFs also have unique mechanical and chemical properties that have motivated the search for applications in composite materials. Adding CNFs to polymers induces electrical conductivity [6]. For catalytic applications, CNFs are attractive materials because these materials form aggregates with high surface areas (100–200 m^2/g), high pore volumes (0.5–2 cm^3/g) without the presence of micropores, and very large external surface areas due to extreme surface roughness [7]. These properties are favorable for a catalyst support material, because sufficient surface area is provided in combination with high porosity and low

* Corresponding author. Fax: +31 534894683.

E-mail address: l.lefferts@tnw.utwente.nl (L. Lefferts).

tortuosity, thus maximizing the effective diffusion coefficient. This is particularly important in the application of heterogeneous catalysts in liquid phase.

Serp et al. [9] recently reviewed the use of CNFs as catalyst supports. Main advantages of CNFs, besides the favourable morphology described above, are high purity of the fibers (preventing poisoning of the active phase by impurities in the support), chemical stability against acids and bases, high mechanical strength, relatively efficient heat transfer, and the occurrence of specific metal–support interactions, offering a way to modify the catalytic performance, as demonstrated in a number of conversions [10–14].

CNFs as such cannot be handled in reactors because of the pressure drop in fixed-bed reactors and tedious filtration in slurry operation. One way to solve this problem is to prepare aggregates with well-controlled particle sizes, as was done by Theunissen [15], Winter et al. [16], and Van der Lee et al. [17]. Small particles for slurry phase operation are not available, however; moreover, filtration would still be necessary. Consequently, several concepts to immobilize CNFs on structured materials, such as graphite felts [18], carbon black [19], Incoloy filter materials [20], and monolith-shaped porous ceramic supports, are currently under study in our lab [21].

The option considered in this work is the application of Ni foams as structured support for CNFs. Like in the work on Incoloy filters [20], CNFs can be grown directly without an additional step to introduce the catalyst to grow CNFs (e.g., Ni), as is necessary when starting from carbon-based materials. Furthermore, the macroscopic structure of foams is very regular, and the hydrodynamic properties have already been studied in detail [22]. Application of Ni instead of a Ni–Fe-based alloy will probably influence the morphology of the resulting material. Finally, recent work of Tribolet [20] has demonstrated the possibility of depositing Pd on CNFs despite the presence of a metallic macroscopic support material.

In a previous study [23] we showed that the formation of CNFs on polycrystalline Ni foams started with fragmentation of the Ni grains into small (i.e., nanosized) particles. This was recently supported by the work of Vieira et al. [18], who reported that many CNFs grew from a single 1- μm Ni particle. It is essential to precisely control the rate of formation as well as the amount of CNFs via the experimental conditions to obtain CNFs that are well attached to the Ni surface, as we described previously [23]. Overabundant formation of CNFs causes complete disintegration of the Ni foam due to corrosive metal dusting. It was also shown that CNFs account for >95% of the carbon deposited on the foam. In the present study we explored the possibility of manipulating the yield, the attachment to the foam, and the morphology of CNFs by modifying the surface morphology of the Ni foam. We also studied the initiation of CNF formation by following the changes in surface morphology of the Ni foam with time of formation in an attempt to improve our understanding of the mechanism of CNF formation on polycrystalline Ni.

2. Experimental

2.1. Materials

The Ni foam (<99 wt% Ni according XRF, obtained from RECEMAT) applied in this study is a three-dimensional network of connected strands [22]. The apparent density of the foam varied within the sheet ($\pm 25\%$) due to variation in the thickness of the walls of the hollow strands. The geometric surface area per gram of Ni was estimated as <1 m²/g. Hydrogen and nitrogen (99.999%, INDUGAS) and ethene (99.95%, PRAXAIR) were used for CNF formation without further purification.

2.2. CNF formation

CNF formation was carried out in a quartz reactor with a porous quartz plate at the bottom to support the Ni foam. Cylindrical samples of Ni foam (10 mm i.d., 5 mm long) were prepared using wire-cut electrical-discharge machining (AGIECUT CHALLENGE 2). A sample of about 0.4 g was used to form the CNFs. Three pretreatment procedures were used. First, samples were reduced at 500 or 700 °C in 20% H₂ in N₂ with a total flow rate of 100 mL/min. The temperature was raised at a rate of 5.5 °C/min from room temperature to the reduction temperature (2 h dwell time). The reduced samples are designated as (red- and reduction temperature in °C). Second, samples were oxidized in stagnant air at 300–700 °C. The temperature was raised at a rate of 10 °C/min from room temperature to the oxidation temperature (1 h dwell time). The oxidized samples are designated as (oxid- and oxidation temperature in °C). Third, Ni foam was oxidized in stagnant air at 700 °C for 1 h as described above and then reduced in 20% H₂ in N₂ with total flow rate of 100 mL/min at 700 °C for 2 h dwell time. This sample was designated as (oxid-700 °C–red-700 °C). After pretreatment, the temperature was increased or decreased in the same gas mixture used for the pretreatment (5 °C/min) to 450 °C to form CNFs for growth times between 0.5 and 2 h, using 25% C₂H₄ in N₂ with a total flow rate of 107 mL/min (0.45 s of contact time). The overall C/Ni ratio varied between 0.18 and 0.72 mol_C/g_{Ni}.

Ethene conversion was determined every 2 min with on-line gas chromatography (Varian 3700 equipped with a 15-m Q-Plot column). The formation rate was calculated from the production rate of hydrogen, which was the only significant product detected in the gas phase. The maximum conversion of ethene was always <10% unless a higher conversion is reported.

Finally, the sample was cooled in N₂ to room temperature. The results reported here are fully reproducible provided that one batch of Ni foam is used, due to inhomogeneity in the Ni foam, as explained in the Materials section.

2.3. Characterization

After CNF formation, samples were cleaned from any loose CNFs by blowing 100 L/min air stream at room temperature for 1 min through the foam before further characterization. This

treatment was done to remove a small fraction of loose fibers; no further fiber loss occurred when the treatment was repeated.

Surface concentration of C on the fresh and reduced Ni foams was measured with X-ray photoelectron spectroscopy (XPS; Physical Instruments Φ Quantum 2000). The structure of the samples during exposure to ethylene was studied *ex situ* with X-ray diffraction (XRD) and scanning electron microscopy (SEM). The samples were allowed to cool in ethylene to about 30 °C before being exposed to air; then the samples were transferred to the spectrometer or microscope. XRD measurements were started within 30 min, and the SEM pictures were taken the next day. XRD was performed using a PANalytical X'pert-APD powder diffractometer system equipped with a position-sensitive detector with a 2θ range of 120° using Cu- $K_{\alpha 1}$ ($\lambda = 1.78897 \text{ \AA}$) radiation. SEM was done with a LEO 1550 FEG equipped with an EDX analyzer. Many micrographs were taken; only representative micrographs are shown herein. An in-lens detector was used to study CNF morphology. An SE2 detector, which is more sensitive to the higher-energy secondary electrons, was used to determine the distribution of Ni in the surface of the foam. BET surface areas of the CNFs were calculated from the N_2 -adsorption isotherm, obtained at 77 K, using a Micromeritics ASAP 2400.

3. Results

3.1. Effect of pretreatment on the surface morphology of Ni foam

3.1.1. Reduction

The micrographs in Fig. 1 show that pretreatment in hydrogen at temperatures up to 700 °C did not influence the crystallite size on the surface. Crystal size was on the order of 1–10 μm (Figs. 1a and b). However, the high-magnification micrograph in Fig. 1c shows formation of some facets after high-temperature treatment in hydrogen. No facets were observed on the foam as received (not shown).

3.1.2. Oxidation

The representative micrographs in Fig. 2 show typical surface morphology of the Ni foam after oxidation in stagnant air for 1 h at different temperatures. Three-dimensional NiO features were formed on the Ni surface after oxidation at 300 °C, as shown in Fig. 2a. Some of these features were small (20–40 nm) as pointed by (1), while much larger features in the order of microns were seen, as pointed by (2). Fig. 2b shows that most of the surface of the Ni foam is covered with a rough layer after oxidation at 500 °C, whereas some areas of the Ni foam seem bare, as pointed out in (1). Figs. 2c and d show a rough, macroporous layer completely covering the surface after oxidation at higher temperatures. However, oxidation of Ni foam at 700 °C resulted in a smoother surface (Fig. 2d); the NiO layer appears dense but still comprises NiO crystallites <100 nm.

These samples were also characterized with XRD, as shown in Fig. 3. Three Ni metal peaks were detected at 2θ positions of 44.5, 51.9, and 76.4°. Three main NiO peaks were detected at 2θ positions of 37.3, 43.3, and 62.9°. The intensities of the NiO

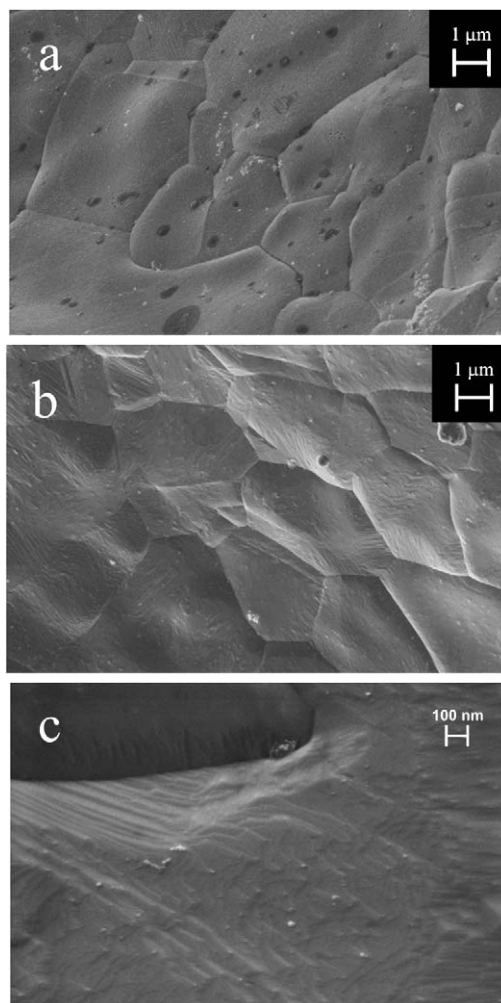


Fig. 1. SEM micrograph of the surface of Ni foam: (a) as received, (b, c) after reduction in 20% H_2 (balance N_2) at 700 °C.

peaks increased with oxidation temperature. NiO wt% was estimated using the reference intensity ratio method [24], and NiO grain sizes were estimated using the Scherrer equation on the diffraction peak at 43.3°. The data in Table 1 show that the estimated NiO wt% from the XRD data is in fair agreement with the NiO wt% calculated from the weight increase of the samples during oxidation. Moreover, it shows that both the weight percentage of NiO and the average size of the NiO grains increased with increasing oxidation temperature. XRD detected no NiO on samples oxidized at 300 °C. The trends in the NiO crystallite sizes observed with XRD, as well as the order of magnitude, agree well with the SEM observations in Fig. 2.

3.1.3. Oxidation followed by reduction

Fig. 4 shows a rough Ni surface containing pits after oxidation and subsequent reduction, both at 700 °C. Obviously, reduction of the NiO layer resulted in the formation of new Ni grains that are considerably smaller than the original grains (1–10 μm) in the as-received material (Fig. 1a). On the other hand, the Ni crystallites formed here are considerably larger than the NiO crystallites observed after the oxidation treatment (Fig. 2d).

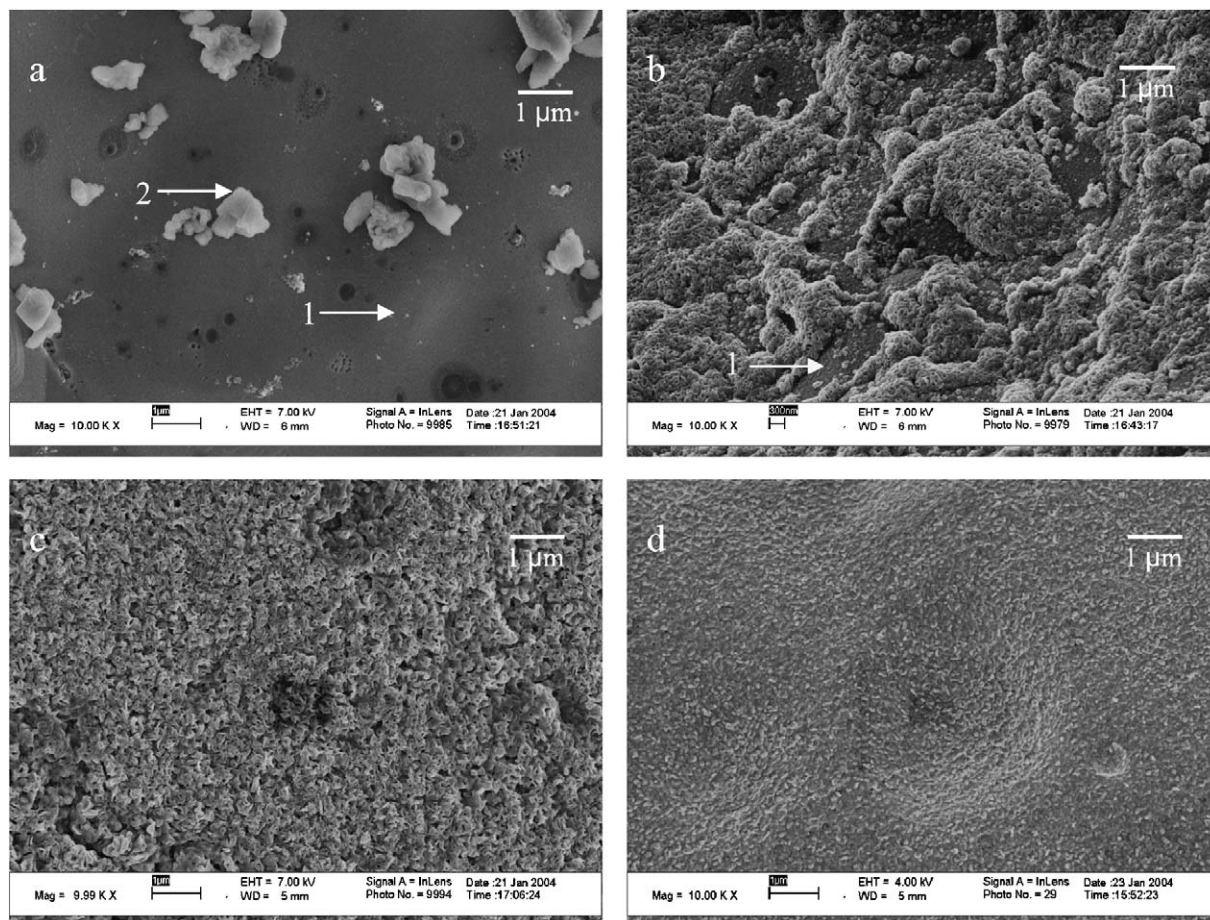


Fig. 2. SEM micrographs of the surface of Ni foam after oxidation at different temperatures in static air for 1 h: (a) oxid-300 °C, (b) oxid-500 °C, (c) oxid-600 °C, and (d) oxid-700 °C.

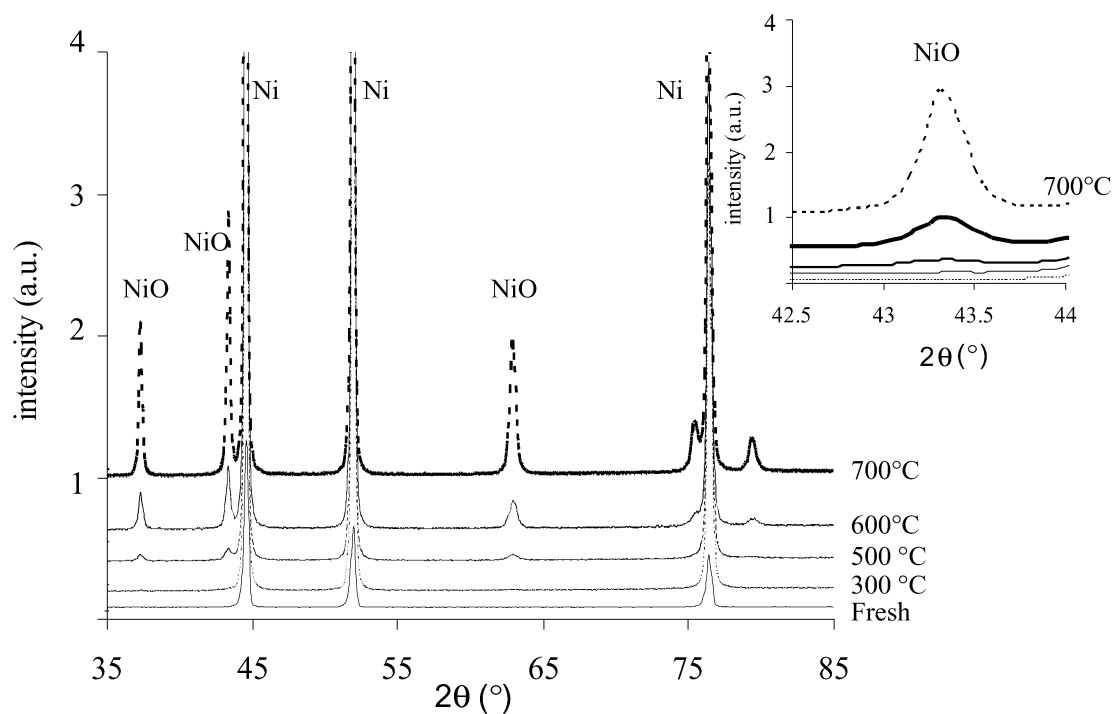


Fig. 3. X-Ray diffraction patterns of Ni foam oxidized in static air for 1 h at different temperatures; insert shows the peak shape of the main NiO reflection.

Table 1

Amount of NiO after oxidation of Ni foam and the average size of the NiO crystallites as estimated from XRD peak intensity and line-broadening using the NiO peak at 43.3°

Sample	NiO (wt%) (XRD)	NiO (wt%) (weight increase)	Average size of NiO grains (nm)
Oxid-500 °C	1	2 (±0.6)	28
Oxid-600 °C	4	3 (±0.3)	41
Oxid-700 °C	18	15 (±0.05)	76

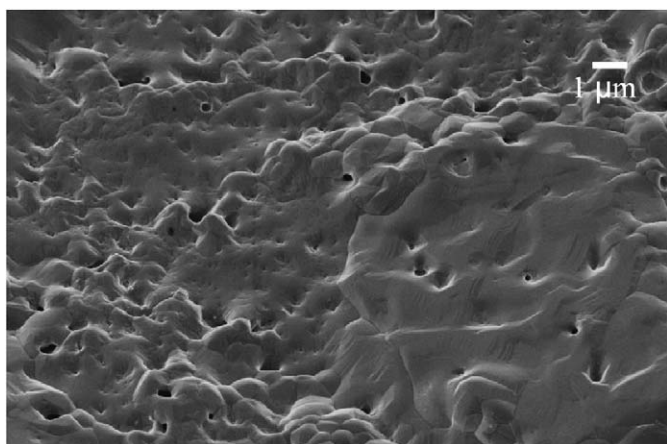


Fig. 4. SEM micrograph of the surface of the Ni foam after oxidation at 700 °C in static air followed by reduction in 20% H₂ (balance N₂) at 700 °C.

In summary, the pretreatments applied here resulted in three types of morphologies of the Ni foam: reduced Ni foam with grain size of 1–10 μm (Fig. 1), rereduced Ni foam with smaller grains (Fig. 4), and oxidized Ni foam covered with varying amounts of NiO grains, ranging in size from 30 to 70 nm (Table 1).

3.2. Effect of pretreatment on the rate of CNF formation

The CNF formation rate as a function of time is shown in Fig. 5; the data were calculated from the rate of hydrogen formation as determined from the analysis of the exit gas stream every 2 min. We discuss the validity of this approach later in the paper. High-temperature reduction clearly decreased the rate of CNF formation and increased the inhibition time. Fig. 5a also shows that the CNF formation rate was higher in the sample oxidized before reduction compared with the sample reduced at 700 °C without previous oxidation.

Fig. 5b shows that the CNF formation rate increased with oxidation temperature; the foam was not prerduced with H₂ in these experiments. The initiation of CNF formation was faster on the oxidized samples (Fig. 5b) than on the prerduced samples (Fig. 5a). Note that the formation rate was one order of magnitude higher on the oxidized samples (Fig. 5b) than on the prerduced samples (Fig. 5a).

Table 2 gives the final amount of CNFs of the samples as determined directly from the increase in weight, as well as estimated from the rate of hydrogen formation. The data are in reasonable agreement.

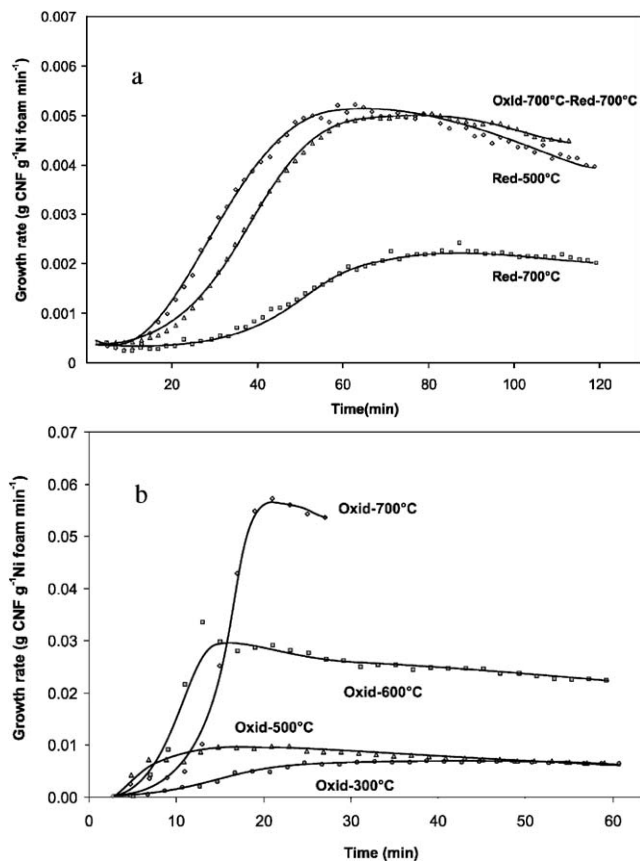


Fig. 5. The formation rates of CNFs as a function of time on (a) reduced Ni foam and (b) Ni foam oxidized at different temperatures. Conditions of CNF formation: 25% C₂H₄ in N₂ (total flow rate 107 ml/min) at 450 °C.

Table 2

Concentration of CNFs formed on Ni foam during exposure at 450 °C during exposure time as indicated; foam samples pretreated at different conditions as indicated; CNF loadings were calculated based on the weight increase directly and based on ethylene consumption as estimated from the rate of H₂ production

Sample (growth time)	Weight increase (%)	Weight increase based on H ₂ formation (%)
Red-500 °C (125 min)	37.5	45.0
Red-700 °C (167 min)	23.3	25.7
Oxid-700–Red-700 °C (2 h)	n.a.	38
Oxid-300 °C (1 h)	n.a.	30
Oxid-500 °C (113 min)	86.8	74.7
Oxid-600 °C (1 h)	n.a.	74
Oxid-700 °C (30 min)	n.a.	131

The most active foams (oxidized at 600 and 700 °C without prerduction with H₂) collapsed completely during CNF formation at 2 and 1 h, respectively, leaving only powder of Ni and CNFs. All other samples remained intact. Fig. 6a is a representative micrograph showing the details of the CNFs formed on stable samples. The CNF diameter was 40–70 nm. In contrast, Fig. 6b shows a typical micrograph of CNFs formed on collapsed foam. Again, CNFs with diameters of 40–70 nm are observed, but much smaller CNFs were also present, as indicated by the circles in Fig. 6b. The BET surface area of foams loaded with CNFs was 90 ± 10 m²/g in all samples, regardless of pretreatment conditions.

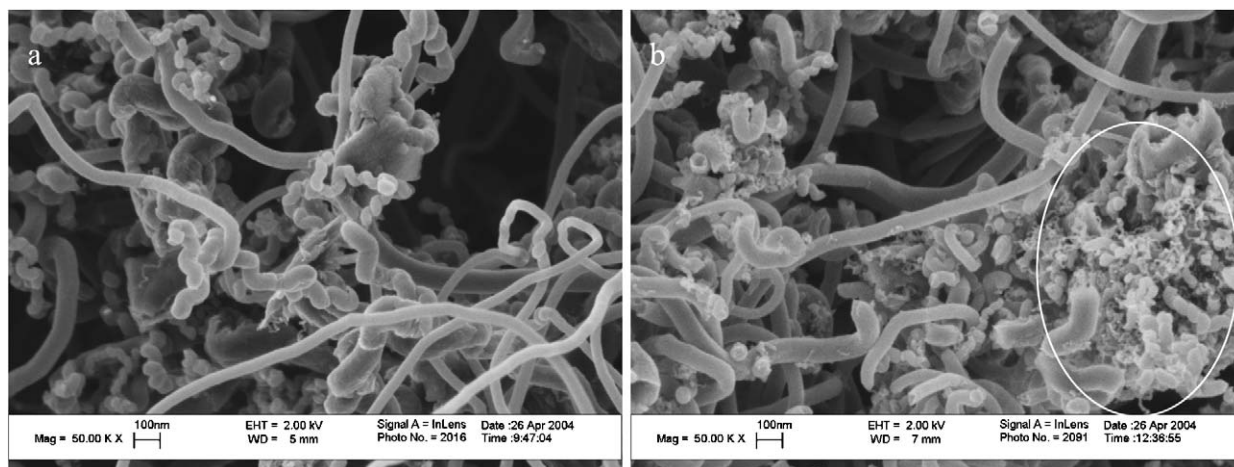


Fig. 6. SEM micrographs of CNFs formed on Ni foam during exposition to 25% C_2H_4 in N_2 at 450 °C. (a) Ni foam oxidized at 500 °C (exposure during 2 h, Ni foam did not collapse) and (b) Ni foam oxidized at 700 °C (exposure during 1 h, Ni foam collapsed).

3.3. Effect of the time of formation on CNF Formation

The initiation of CNF formation on Ni foam was investigated by exposing Ni foam to the gas mixture (ethene and N_2) for short periods. Changes in the surface morphology of the foam as a result of the exposure to the gas mixture were observed with *ex situ* SEM as well as XRD. The Ni foam reduced at 700 °C was chosen for this part of the study because the slow kinetics of CNF formation (Fig. 5a) allows observation of the changes on the Ni surface before achievement of complete coverage with CNFs.

The micrographs in Fig. 7 show the changes in the surface morphology of the Ni foam after different reaction times. Fig. 7a shows that rectangular-shaped features (strips) with a dimension of 100×200 nm were formed on the surface of the Ni foam after 1 min of reaction at 450 °C. After 5 min of reaction, the strips developed into slightly larger features, and a very limited number of CNFs were observed (Fig. 7b). The morphology of the Ni surface did not change significantly after 10 min of reaction (not shown). More CNFs were formed and accumulated on the surface of the foam after 20 min (Fig. 7c). Fig. 7d shows the surface of the Ni foam after 30 min of reaction. The left side of this micrograph was taken using the inlens detector, and the right side was taken using the SE2 detector. The left side of the micrograph shows a very rough surface with some CNFs, whereas the right side shows small Ni particles (20–100 nm) on the surface of the foam. CNFs and fragmented Ni particles were observed on the surface of the Ni foam after 1 and 2 h of CNF formation, respectively, as shown in Figs. 7e and f. Some of these Ni nanoparticles are located in or at the top of CNFs.

Fig. 8a shows a series of XRD patterns of Ni foams reduced at 700 °C and after 10 and 120 min of CNF formation. The patterns in Fig. 8a show five Ni metal diffraction peaks at 2θ positions between 40 and 100°. Neither the shape nor the intensity of these peaks varied with the formation time. A graphite peak was recorded after 120 min of CNF formation at 2θ of 26°. Fig. 8b shows that the graphite peak can be observed only after at least 1 h of formation. On the other hand, four peaks with low intensities were detected at 2θ positions of 39.3, 41.6,

58.6, and 72.3° after 10 min of CNF formation, as indicated by the rectangles in Fig. 8c. These diffraction peaks can be assigned to the Ni_3C that began to form after 1 min of exposure, as shown by the circles in Fig. 8c. The intensity of the Ni_3C peaks continues to increase in the first 10 min of CNFs formation, where after the Ni_3C peaks completely disappeared after 20 min of reaction.

4. Discussion

First, we discuss the initiation of CNF formation by following the change in the morphology of Ni over time. Then we discuss the effect of surface morphology of the Ni foam on the CNF structure and rate of formation.

4.1. Initiation

Exposure to ethylene for 1 min at 450 °C induced the formation of strip-shaped crystallites (Fig. 7a) at the surface of the Ni foam that originally appeared very smooth (Fig. 1c). The size of these crystallites seemed to increase somewhat after 5 min (not shown) and 10 min (Fig. 7b). The XRD spectra in Fig. 8c demonstrate that Ni_3C was detected in exactly the same window of time of exposure, in contrast to longer times of exposure.

It is well known that Ni_3C is not stable against air. Nevertheless, the XRD data indicate that at least part of the Ni_3C phase survived the relatively short exposure to air at room temperature. It is therefore also reasonable to propose that the crystallites at the surface also consist of Ni_3C , or at least their particular shape is due to Ni_3C decomposition in air.

XRD results in Fig. 8c show that longer exposure to ethylene does not result in the detection of any Ni_3C , whereas both the SEM micrographs in Fig. 7 and the rates of CNF formation in Fig. 5a (red-700 °C) indicate that CNF formation was just starting after 20–30 min. Fig. 7c clearly shows that CNF formation began on extremely rough surfaces, and Fig. 7d demonstrates that small Ni particles were formed. Fig. 7e clearly indicates that after longer exposure, at least part of the CNFs contained Ni in the fibers, either in the top or somewhere in the middle.

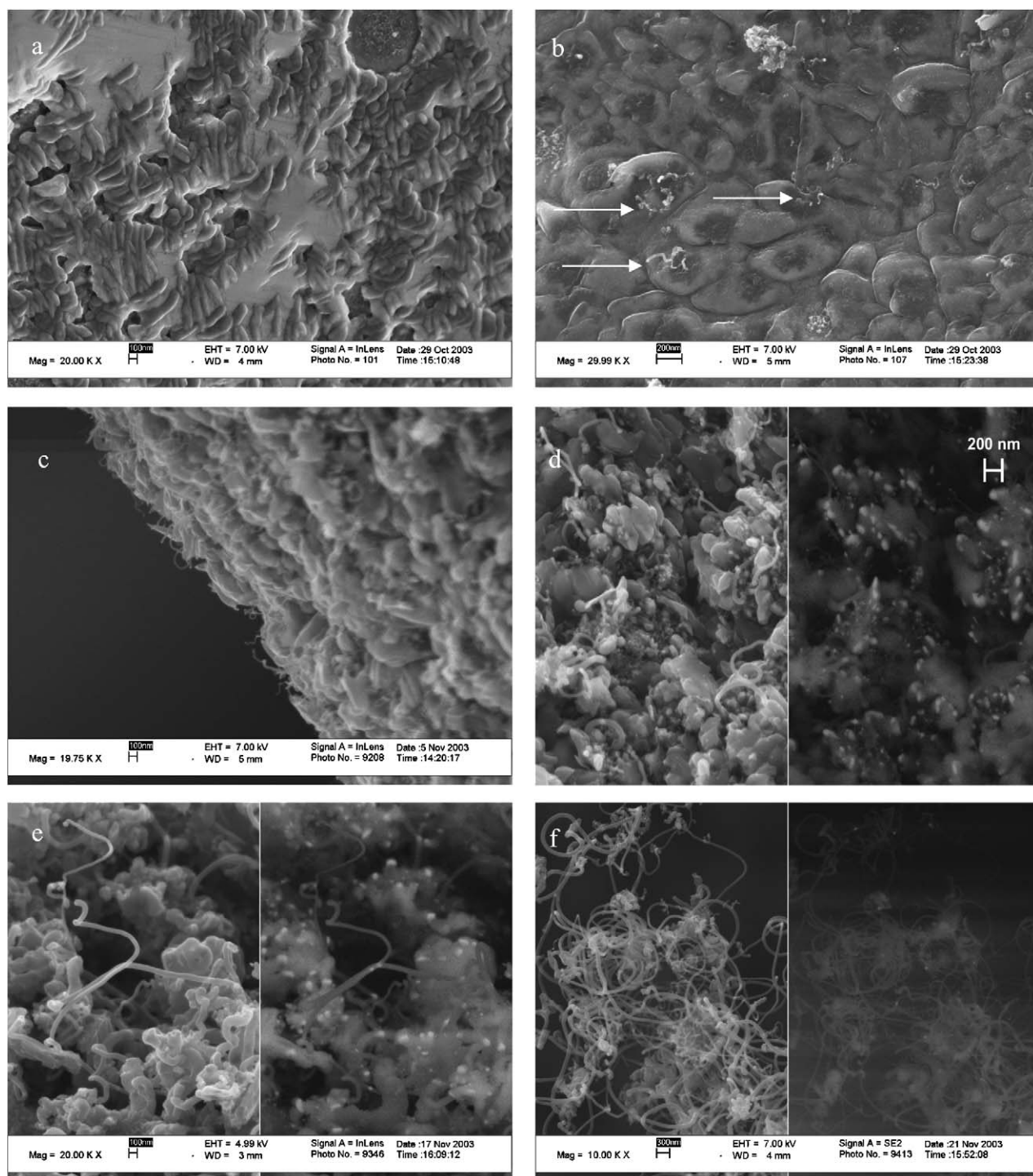


Fig. 7. SEM micrographs of the surface of Ni foam (reduced at 700 °C) after exposure to 25% C₂H₄ in N₂ (total flow rate 107 mL/min) at 450 °C during (a) 1 min, (b) 5 min, (c) 20 min, (d) 30 min, (e) 60 min, (f) 120 min; in the right-hand panels in micrographs (d), (e), and (f) Ni particles show bright.

Our previous study provides more detailed evidence of this effect [23]. In conclusion, the original large (> 1 μm) Ni crystals were first converted to Ni₃C at the surface, which then allowed the formation of Ni nanoparticles (20–70 nm), which facilitated CNF formation.

A comparable SEM approach to identifying the initiation of CNF formation was followed by Park and Keane [25] for supported preshaped Ni particles. To the best of our knowledge,

our work is the first to study the initiation of CNF formation on polycrystalline nickel with microscopy. It is generally accepted that the formation of CNFs out of preshaped, supported Ni nanoparticles is preceded by the formation of Ni₃C [26–30]. Our study is the first to directly prove the formation of Ni₃C, preceding CNFs formation on polycrystalline Ni. Two factors enabled the detection of Ni₃C on polycrystalline Ni in this study. First, the surface area of the Ni foam was two orders of

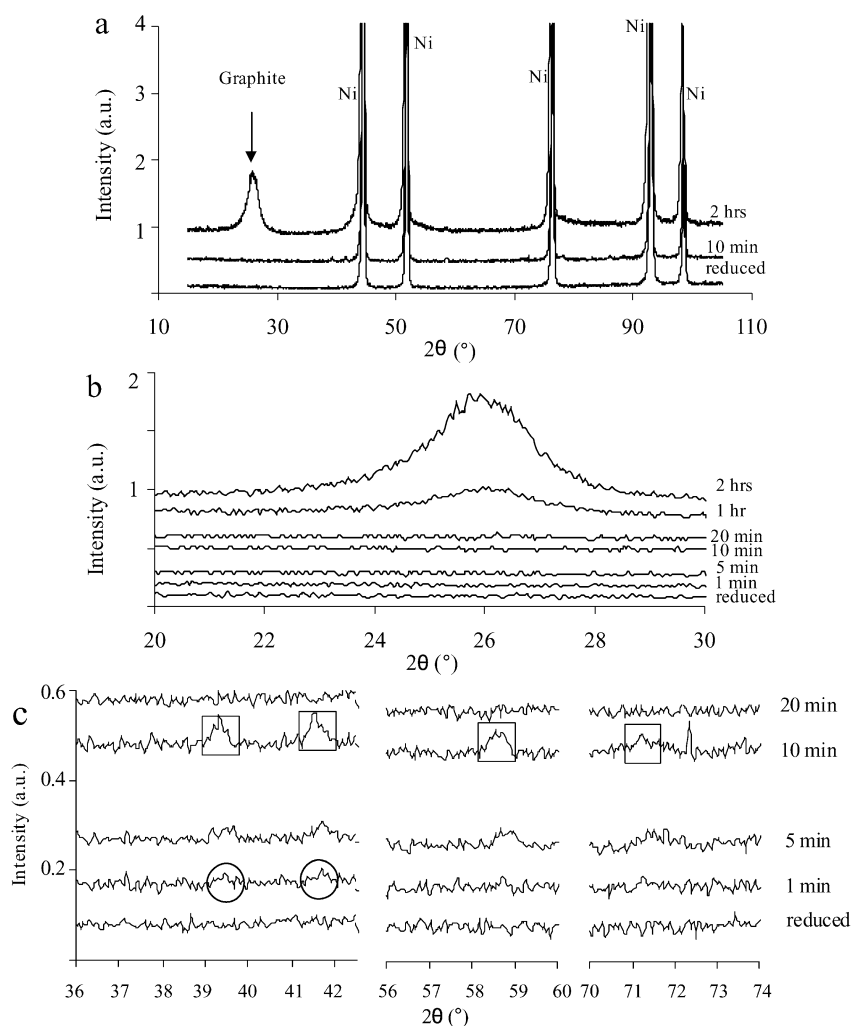


Fig. 8. X-Ray diffraction patterns on Ni foams (reduced at 700 °C) after exposure to 25% C₂H₄ in N₂ (total flow rate 107 mL/min) at 450 °C during 0, 10 and 120 min; (a) overview diffraction pattern, (b) graphite reflection, and (c) Ni₃C reflections.

magnitude greater than that of the polycrystalline Ni used previous studies [31–33]. Second, the time window within which Ni₃C can be observed was maximized in this work by minimizing the rate of CNF formation, selecting a suitable pretreatment of the foam, and using a lower formation temperature (i.e., 450 °C). Similarly, Goodman et al. [34] studied the kinetics of Ni₃C formation on Ni(100) using Auger electron spectroscopy and found that the decomposition of Ni₃C and formation of graphite started after <10 s at 527 °C, whereas the initiation of graphite formation took 4 min at 427 °C. This finding is in fair agreement with our SEM results showing formation of a limited amount of CNFs after 5 min of reaction at 450 °C (Fig. 7b). Renshaw et al. [35] and Chun et al. [36] used transmission electron microscopy to study CNF formation on polycrystalline Ni and suggested that the observed hexagonal close-packed structures on the Ni surface were due to formation of Ni₃C. Nakano et al. [37] also found proof for the formation of Ni₃C using scanning tunnelling microscopy, Auger electron spectroscopy, and low-energy electron diffraction, although at much lower temperatures (227–327 °C). These results are in line with our observations.

4.2. CNF morphology

The BET surface area of the carbon deposited on the Ni foam was 90 (±10) m²/g_{carbon}. Our previous study found that, based on temperature-programmed hydrogenation, at least 95% of the carbon deposited is CNFs [23]. Thus we can conclude that the surface area of the CNFs is also 90 m²/g. This value is at the lower end of typical surface areas of CNFs reported in the literature, which range from about 100 to 250 m²/g. These values were achieved with supported Ni catalysts, and it is obvious that the particle sizes of the active Ni particles may be very different in our case. Surprisingly, Tribollet and Kiwi-Minsker [38] have reported much higher values (up to 500 m²/g) when growing CNF on Ni, stainless steel, and Incoloy; this is possibly due to differences in the conditions and/or the composition of the Incoloy instead of the Ni.

The mean diameter of the CNFs that follows from the surface area, assuming absence of any microporosity and assuming that the density of the CNFs equal to the density of graphite, 2.3 g/cm³ [7,39], is 22 ± 2 nm. At first glance, this seems to disagree with the observation of CNFs with diameter of 40–70 nm

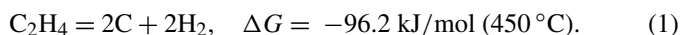
on stable foam (Fig. 6a); however, Fig. 6b reveals that disintegrated materials with very high amounts of CNFs (>50% by weight) contain CNFs with a much broader distribution of diameters. We are thus inclined to conclude that all samples must contain CNFs with a broad distribution of diameters, although the thin fibers are not visible at the outer surface of the CNF layer.

Huang et al. [40] reported even thicker CNFs (100–300 nm) on the surface of a Ni foam using acetylene and high temperature (550–700 °C). The differences are probably due to the different conditions.

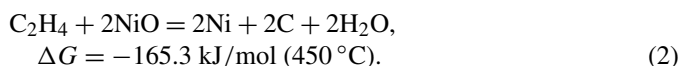
According to the XRD results (Fig. 8b), the CNFs consist of graphite layers with an interlayer spacing similar to that of bulk graphite (i.e., 0.34 nm) [15,41]. The peak shape in Fig. 6 is rather broad, indicating poor crystallinity [40], as would be expected at the relatively low temperatures used.

4.3. Rate of CNF formation

In this study the rates of CNF formation have been calculated based on the rate of H₂ formation, according to the following formula:



This is allowed because no other products, such as methane or ethane, were formed in any significant amounts. However, in the presence of NiO, the following reaction can be anticipated:



H₂ is effectively consumed to reduce NiO. We cannot provide solid evidence of this, because the water concentration in the exit gas could not be determined. However, the formation of CO and CO₂ instead of water can be excluded. Reaction (2) would cause underestimation of the rate of CNF formation calculated from the rate of H₂ formation; however, it can be calculated that the error thus introduced is just 3% by weight for the foam oxidized at 700 °C (containing 15 wt% NiO); this error is insignificant compared with the CNF concentration (131%). The error for the samples oxidized at lower temperatures is even smaller, whereas the reduced samples contain no NiO at all. Nevertheless, the peculiar observation that foams with high NiO content have even lower initial activity (Fig. 5) is possibly an artifact caused by H₂ consumption through NiO reduction.

The rate of CNF formation is determined by two factors: the number of Ni particles that allow CNF formation and the intrinsic rate of CNF formation for each Ni particle. The average diameter of the Ni particles contributing to CNF formation is constant based on the invariant surface area of the CNFs (expressed per gram of carbon), as discussed in Section 4.2. Furthermore, the conditions applied in CNF formation were identical in all experiments in this study (i.e., 450 °C, C₂H₄). A detailed discussion of the rate-determining step is beyond the scope of this work; nevertheless, the intrinsic rate of CNF formation per Ni particle can thus be assumed to be constant. In other words, the difference in the observed rates of CNF formation must be due to different numbers of active Ni particles present.

Fig. 5a shows that the rate of CNF formation on polycrystalline Ni with large grain sizes (red-700 °C) is lower than the rate on Ni with smaller grain sizes (oxid-700 °C–red-700 °C). Apparently, Ni nanoparticles are formed more rapidly from smaller Ni crystals. This can be tentatively explained by assuming that the sequence of Ni₃C formation and subsequent decomposition to Ni nanoparticles is enhanced at grain boundaries, a reasonable assumption, because it is well known that carbon dissolved in Ni segregates at grain boundaries [31].

Unexpectedly, the presence of NiO increased the rate of CNF formation by one order of magnitude, as shown in Fig. 5. In contrast, metal oxides have been reported to inhibit CNF formation [5,42]. Apparently, reduction of NiO with ethylene under the conditions in the present work induces much greater formation of Ni nanoparticles compared with reduced Ni samples. Generally, reduction of NiO to Ni proceeds through formation of Ni nuclei; these nuclei will grow, and we speculate that these nanoparticles are able to contribute to CNF formation when at roughly 20–70 nm. Whether or not Ni₃C is involved in this case remains an open question. The essential difference is that Ni nanoparticles are formed rapidly through the reduction of NiO, as opposed to decomposition of a fraction of relatively large Ni₃C crystals as observed on reduced Ni.

The maximum rate of CNF formation increased with oxidation temperature (Fig. 5b). Apparently, the amount of NiO (Table 1) was more relevant than the size of the NiO crystallite (Fig. 2 and Table 1), possibly due to the fact that all oxidized samples contained relatively small NiO crystals.

Our results are in agreement with those of Baker et al. [43], who reported that CNF formation using ethane and acetylene was one order of magnitude faster on FeO than on Fe. These authors attributed this effect to the high surface area of the Fe that formed during reduction of FeO. Moreover, formation of H₂O during the decomposition of C₂H₄ on NiO, instead of H₂ on Ni, would shift the equilibrium of reaction (2), compared with reaction (1), in the direction of Ni₃C formation [44], and consequently, more rapid CNF formation would be expected. Unfortunately, the present study could not confirm this effect, because the formation of water was not investigated. In any case, the rate of CNF formation increased by one order of magnitude as shown in Fig. 5, and this effect is clearly too large to be attributed exclusively to surface area.

It should be noted that the ratio of CNFs formed and the amount of Ni used was very low compared with that found in experiments with metal powders (up to 300 g of carbon per g of metal) [25] with the intent to maximize the C/Ni ratio, because in our work most of the Ni should remain within the foam network to ensure sufficient mechanical stability of the metallic backbone of the Ni foam.

5. Conclusion

This study explored how the formation of CNFs from ethene begins on polycrystalline Ni. The effect of the morphology and surface properties (i.e., grain size and the presence of NiO) on CNF formation was studied in detail. The formation of CNFs

on polycrystalline Ni starts with the formation of meta-stable Ni_3C , which later decomposes into Ni and C. As a result, Ni nanoparticles are formed with the proper dimension (20–70 nm) to facilitate formation of CNFs. Consequently, the rate of CNF formation on polycrystalline Ni becomes significant after decomposition of Ni_3C , forming sufficient Ni nanoparticles. Grain boundaries in the parent Ni material appear to enhance this process. The presence of NiO increases the rate of CNF formation by one order of magnitude. NiO is reduced in situ, and Ni nanoparticles are formed directly, as opposed to the sluggish formation of Ni nanoparticles through the decomposition of Ni_3C particles from relatively large (1–10 μm) Ni crystals.

References

- [1] M. Rodriguez, *J. Mater. Res.* 8 (12) (1993) 3233.
- [2] T. Ros, *Rhodium Complexes and Particles on Carbon Nanofibers*, Thesis, Utrecht, 2002.
- [3] F. Bonnet, F. Ropital, Y. Berthier, P. Marcus, *Mater. Corros.* 54 (11) (2003) 870.
- [4] D.L. Trimm, *Catal. Rev.-Sci. Eng.* 16 (1977) 155.
- [5] C.H. Bartholomew, *Catal. Rev.-Sci. Eng.* 24 (1982) 67.
- [6] R.T. Baker, P.S. Harris, R.B. Thomas, R.J. Waite, *J. Catal.* 30 (1973) 86.
- [7] K.P. de Jong, J.W. Geus, *Catal. Rev.-Sci. Eng.* 42 (2000) 481.
- [8] S. Iijima, *Nature* 354 (1991) 56.
- [9] P. Serp, M. Corrias, P. Kalck, *Appl. Catal. A: Gen.* 253 (2003) 337.
- [10] C. Huu, N. Keller, G. Ehret, L. Charbonniere, R. Ziessel, M. Ledoux, *J. Mol. Catal. A* 170 (2001) 155.
- [11] R. Vieira, C. Pham-Huu, N. Keller, M.J. Ledoux, *Chem. Commun.* (2002) 454.
- [12] M.J. Ledoux, C. Pham-Huu, *Catal. Today* 2 (2005) 102–103.
- [13] M.L. Toebes, T.A. Nijhuis, J. Hajek, J.H. Bitter, A.J. van Dillen, D.Y. Murzin, K.P. de Jong, *Chem. Eng. Sci.* 60 (2005) 5682.
- [14] C. Park, M.A. Keane, *J. Colloid. Interface Sci.* 266 (2003) 183.
- [15] W. Teunissen, *Tailoring of Carbon Fiber and Carbon-Coated Ferromagnetic Catalyst Supports*, Thesis, Utrecht University, 2000.
- [16] F. Winter, V. Koot, A.J. van Dillen, J.W. Geus, K.P. de Jong, *J. Catal.* 236 (2005) 91.
- [17] M.K. van der Lee, A.J. van Dillen, J.W. Geus, K.P. de Jong, J.H. Bitter, *Carbon* 44 (2006) 629.
- [18] R. Vieira, M.J. Ledoux, C. Pham-Huu, *Appl. Catal. A* 274 (2004) 1.
- [19] S. Lim, S.H. Yoon, Y. Korai, I. Mochida, *Carbon* 42 (2004) 1765.
- [20] P. Tribolet, L. Kiwi-Minsker, *Catal. Today* 105 (2005) 337.
- [21] N. Jarrah, J.G. van Ommen, L. Lefferts, *J. Mater. Chem.* 14 (10) (2004) 1590.
- [22] C.P. Stemmet, J.N. Jongmans, J. van der Schaaf, B.F.M. Kuster, J.C. Schouten, *Chem. Eng. Sci.* 60 (2005) 6422.
- [23] N. Jarrah, J.G. van Ommen, L. Lefferts, *J. Mater. Chem.* 15 (2005) 1946.
- [24] R. Jenkins, R.L. Snyder, *Introduction to X-Ray Powder Diffractometry*, Wiley, New York, 1996, pp. 370–374.
- [25] C. Park, M.A. Keane, *Langmuir* 17 (2001) 8386.
- [26] P.K. Bokx, A.J. Kock, E. Boellaard, W. Klop, J.W. Geus, *J. Catal.* 96 (1985) 454.
- [27] N.C. Triantafyllopoulos, S.G. Neophytides, *J. Catal.* 217 (2003) 324.
- [28] J. Kock, P.K. Bokx, A.E. Boellaard, W. Klop, J.W. Geus, *J. Catal.* 96 (1985) 468.
- [29] M.S. Hoogenraad, Thesis, Utrecht University, 1995.
- [30] A. Barrier, E.B. Pereira, G.A. Martin, *Catal. Lett.* 45 (1997) 221.
- [31] A. Sacco, F.W. Geurts, G.A. Jablonski, S. Lee, R.A. Gately, *J. Catal.* 119 (1989) 322.
- [32] Z. Zeng, K. Natesan, *Chem. Mater.* 15 (2003) 872.
- [33] R. Schneider, E. Pippel, J. Woltersdorf, S. Strauß, H. Grabke, *Steel Res.* 68 (7) (1997) 326.
- [34] D.W. Goodman, R.D. Kelley, T.E. Madey, J.M. White, *J. Catal.* 64 (1980) 479.
- [35] G.D. Renshaw, C. Roscoe, P.L. Walker, *J. Catal.* 22 (1971) 394.
- [36] C.M. Chun, J.D. Mumford, T.A. Ramanarayanan, *J. Electrochem. Soc.* 147 (10) (2000) 3680.
- [37] H. Nakano, J. Ogawa, J. Nakamura, *Surf. Sci.* 514 (2002) 256.
- [38] P. Tribolet, L. Kiwi-Minsker, *Catal. Today* 15 (2005) 102–103.
- [39] R. Weast, *CRC Handbook of Chemistry and Physics*, 64th Ed., CRC Press, Boca Raton, FL, 1983.
- [40] W. Huang, X. Zhang, J. Tu, F. Kong, Y. Ning, J. Xu, G. van Tendeloo, *Phys. Chem. Chem. Phys.* 4 (2002) 5325.
- [41] M. Endo, Y. Kim, T. Takeda, S. Hong, T. Matusita, T. Hayashi, M. Dresselhaus, *Carbon* 39 (2001) 2003.
- [42] M.P. Manning, J.E. Garmlrlan, R.C. Reid, *Ind. Eng. Chem. Res.* 21 (1982) 404.
- [43] R.T. Baker, J.R. Alonzo, J.A. Dumesic, D.J. Yates, *J. Catal.* 77 (1982) 74.
- [44] *Chemical Reaction and Equilibrium Software, HSC Chemistry.*